

NJC

Accepted Manuscript



This is an *Accepted Manuscript*, which has been through the Royal Society of Chemistry peer review process and has been accepted for publication.

Accepted Manuscripts are published online shortly after acceptance, before technical editing, formatting and proof reading. Using this free service, authors can make their results available to the community, in citable form, before we publish the edited article. We will replace this *Accepted Manuscript* with the edited and formatted *Advance Article* as soon as it is available.

You can find more information about *Accepted Manuscripts* in the [Information for Authors](#).

Please note that technical editing may introduce minor changes to the text and/or graphics, which may alter content. The journal's standard [Terms & Conditions](#) and the [Ethical guidelines](#) still apply. In no event shall the Royal Society of Chemistry be held responsible for any errors or omissions in this *Accepted Manuscript* or any consequences arising from the use of any information it contains.



Journal Name

ARTICLE

Reduced recombination with optimized barrier layer on TiO₂ in PbS/CdS core shell quantum dot sensitized solar cells

Dinah Punnoose,^a CH. S. S. Pavan Kumar,^b Araveeti Esvar Reddy,^a S. Srinivasa Rao,^a Chebrolu Venkata Thulasi-Varma,^a Soo-Kyoung Kim,^a Hyun Woong Seo,^c Masaharu Shiratani,^c Sang-Hwa Chung,^a and Hee-Je Kim^a

Received 00th January 20xx,
Accepted 00th January 20xx

DOI: 10.1039/x0xx00000x

www.rsc.org/

Fast electron transport and slow interfacial electron recombination are indispensable features for efficient photo-electrodes of quantum dot sensitized solar cells (QDSSCs). This study reports the methodology to prevent recombination losses in lead sulfide QDSSCs. TiO₂ nano-particles were coated with two different insulating oxide materials (MgO and Al₂O₃). A single and double coated barrier layer is used in order to optimize the passivation effect, prevent recombination losses and to obtain high-performance stable QDSSCs when compared to bare TiO₂. Metal oxides with high isoelectric point enhances the quantum dot adsorption and also increases the TiO₂ conduction band edge. The QDSSCs is examined in detail using polysulfide electrolyte and a copper sulfide (CuS) counter electrode. A solar cell based on double coating electrode (MgO/Al₂O₃) yielded excellent performance with an efficiency (η) of 3.25%. Enrichment in electron transport and decrement in the electron recombination are responsible for the enhanced J_{sc} and V_{oc} of the QDSSCs. The electron lifetime with TiO₂/MgO/Al₂O₃ was higher than those with bare TiO₂, TiO₂/MgO, TiO₂/Al₂O₃ and TiO₂/Al₂O₃/MgO leading to more efficient electron-hole separation and slow downs the electron recombination.

1. INTRODUCTION

Dye-sensitized solar cells (DSSCs) with mesoporous TiO₂ electrode using organic sensitizer have attracted momentous interests because of their low production cost and high efficiency.^{1,2} Semiconductor quantum dots (QDs) with a narrow band gap have recently attracted escalating interests in using photo sensitizers as a substitute to DSSCs. Quantum dot sensitised solar cells(QDSSCs) offer new opportunities to generate multiple electron-hole pairs with a single photon and facilitate the transport of hot electrons.³⁻⁷ QDs with tunable band gaps, light absorption

coefficient and high stability are its great features.⁸⁻¹⁴ *In situ* growth methods which includes successive ionic layer adsorption and reaction (SILAR)¹⁵ and chemical bath deposition (CBD)¹⁶ are used. The combinations of QDs lead to higher efficiencies than pure materials.¹⁷⁻²¹ CdS, CdSe, PbS, PbSe, and Sb₂S₃ are frequently used as QD sensitizers in QDSSCs. Lead sulfide QDs which has high absorption coefficient with a tunable band gap, could be more gainful as an effective sensitizer in QDSSCs.²²

The quantized discrete band structures, multiple exciton and theoretical efficiency which are beyond the Shockley-Queisser limit are advantageous for PbS-sensitized QDSSCs.²³ The performance of PbS QDSSCs is greater when compared to other semiconductor QD-based solar cells.^{24,25} A partial passivation layer of CdS above the PbS-sensitized surface of the photo-anode can decrease the recombination of photo injected electrons with the electrolyte and improve the overall performance of the solar cells.²⁶ CdS and PbS leads to better performance due to its

^a Department of Electrical and Computer Engineering, 2, Busandaehak-ro 63beon-gil, Geumjeong-gu, Busan 46241, Korea

^b Department of Physics, Pusan National University, 2, Busandaehak-ro 63beon-gil, Geumjeong-gu, Busan 46241, Korea

^c Department of Electronics, Kyushu University, 744 Motoooka, Nishi-ku, Fukuoka 819-0395, Japan

*Corresponding author: heeje@pusan.ac.kr

Dinah Punnoose and CH.S.S.Pavan Kumar made equal contribution to this work.

reorganized step-wise band-edge levels.²⁷ By tuning their relative band alignment layer of passivized QDs which serves as both light-absorbing layer and as an electron-blocking or hole-extraction layer. The ZnS SILAR coating technique is used to protect QDs from photo corrosion and to suppress electron recombination with the electrolyte. QDSSCs still show comparatively lower conversion efficiencies than those of DSSCs. The low efficiency of QDSSCs is due to its electron recombination, particularly at the interface between the TiO₂/QDs/electrolyte.^{28,29} High band-gap insulating metal oxides such as SiO₂, Al₂O₃, Nb₂O₅, and MgO which are formed like a core-shell are used as interface between TiO₂ and QDs to act as a barrier layer for electron-transfer processes and suppresses the recombination.³⁰⁻³² TiO₂ nanoparticles have been widely investigated since they exhibit interesting optical, electronic and photo-chemical properties.^{33,34} A wide number of applications such as photovoltaic cells, electro-chromic materials, photocatalysis and waste water treatment have become prospective using TiO₂ nanoparticles.³⁵⁻³⁹ Various metal oxides with a high isoelectric point (IEP) are used to boost dye adsorption and increase the TiO₂ conduction band edge.⁴⁰

MgO nanoparticles are advantageous in high temperature resilient insulating materials, fuel-oil additives, liquid crystals, electro-luminescence display panels and fluorescence tubes.⁴¹⁻⁴⁵ Uniting an insulator material (such as MgO and Al₂O₃) with TiO₂ can boost its photo catalytic performance.^{46,47} Bandara *et al.* stated that TiO₂ coated with MgO enhances the photo degradation of eosin by three fold. The reason behind the enhanced activity of TiO₂/MgO compared to pure TiO₂ is that the MgO layer acts as a barrier for charge recombination.⁴⁷ Liu *et al.* have investigated the photo-reduction of CO₂ with water vapor using TiO₂/MgO as a hybrid adsorbent-photo-catalyst.⁴⁸ Enhanced efficiency in solar cells has been achieved by coating a layer of MgO on TiO₂. MgO layer on TiO₂ hinders the recombination of electrons and holes and since MgO is more simple than TiO₂, the carboxylic groups of the organic dyes easily adsorb on the surface thus refining the efficiency of the dye sensitized solar cells.^{49,50} Tachanet *et al.* reported that the MgO coating layer can act as an interface barrier between TiO₂ and QDs to inhibit recombination losses.¹⁷

Al₂O₃ is known to provide a relatively low interface defect density during growth.⁵¹ Its insulating nature can function as an energy barrier to reduce the charge recombination rate in QDSSCs.⁵² However; the barrier layer can also interfere with

charge separation steps necessary for photocurrent collection by electron injection into TiO₂. The insertion of a barrier layer will slow electron injection without substantially affecting the electron injection yield, allowing for devices to assist from decreased recombination without detrimental effects on photocurrent collection.

Herein, we report for the first time, TiO₂ with metal oxides (MgO and Al₂O₃) and sensitized with PbS/CdS and with the application of polysulfide electrolyte, and a CuS counter electrode which was used to block the recombination. The following barrier layers were fabricated on TiO₂: single coating of (a) MgO, (b) Al₂O₃, and double coating of (c) MgO/Al₂O₃ (d) Al₂O₃/MgO. Along with that PbS/CdS sensitized photo-anode can decrease the recombination of photo injected electrons with the electrolyte. The QDSSC performance is enhanced which is attributed due to the better light harvesting ability of PbS quantum dots and makes large accumulation of photo-injected electrons in the conduction band of TiO₂. We have achieved an efficiency of 3.25% which is high for surface modification of TiO₂ solar cells with lead sulfide QDs. The general structure of the QDSSC is shown with details in Fig. 1.

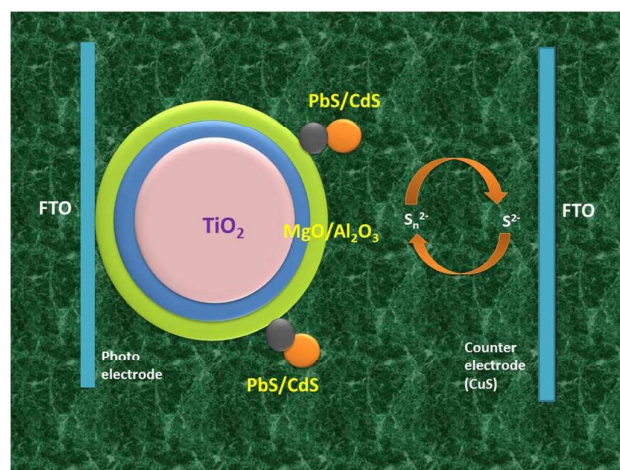


Fig. 1 Graphical representation of Bare TiO₂, TiO₂/MgO, TiO₂/Al₂O₃ and TiO₂/MgO/Al₂O₃ and TiO₂/Al₂O₃/MgO in QDSSCs with CuS counter electrode and polysulfide electrolyte.

The cells are composed of TiO₂ with barrier layer sensitized with QDs the polysulfide electrolyte and CuS counter electrodes. Due to the easy corrosion of the metal chalcogenides in the iodide/triiodide electrolyte, polysulfide is the best choice for QDSSCs. The high band gap insulating materials MgO and Al₂O₃

which are used as an interface between TiO₂ and QDs acts as a barrier layer for electron transfer processes to suppress recombination. Upon 1 sun illumination (100 mWcm⁻²), photons are captured by the QDs, which generate excitons, drive electrons towards the TiO₂ conduction band, and transfers holes to electrolyte. The injected electrons travel through semiconductor and to the back contact, and then through the load to the CE.

2 EXPERIMENTAL SECTION

2.1. Materials

All chemicals used were purchased from Aldrich and employed without any further purification. FTO substrate with a sheet resistance of 10Ω square⁻¹ (Sigma-Aldrich) was used to prepare the photo-anodes and CE. TiO₂ paste (Ti-Nanoxide HT/SP) was supplied by Solaronix.

2.2. Fabrication of PbS/CdS sensitized Bare TiO₂, TiO₂/MgO, TiO₂/Al₂O₃, TiO₂/Al₂O₃/MgO and TiO₂/MgO/Al₂O₃ photo-anodes

With the aim of preparing QDSSCs, a fluorine-doped tin oxide glass (FTO) was used as the substrate for both the photo-anode and CE. TiO₂ photo-anodes were fabricated on an ultrasonically cleaned FTO substrate using the doctor blade method. Anatase TiO₂ particles (Ti-Nanoxide HT/SP, Solaronix) were first deposited on the FTO substrate with an active area of 0.27 cm², followed by sintering at 450 °C for about 30 min. A thickness of ~7 μm was obtained.

The prepared TiO₂ films were immersed into aqueous solutions containing 50 mM aluminum isopropoxide (Al [OCH(CH₃)₂]₃) and magnesium chloride (MgCl₂) coated TiO₂ films. To prepare the double coated barrier layers, such as Al₂O₃/MgO, TiO₂ films were soaked in a (Al[OCH(CH₃)₂]₃) solution and subsequently in a MgCl₂ solution for 15 min each and sintered at 450 °C for 30 min. PbS and CdS QDs were deposited on TiO₂ films by a SILAR technique. The TiO₂ photo-anodes were immersed in a solution containing 25 mM Pb(NO₃)₂ for 5 minutes to allow Pb²⁺ ions to adsorb, and then rinsed with DI water and ethanol to remove the excess Pb²⁺ ions. The photo-anodes were then dipped into an aqueous solution containing 0.1 M sodium sulfide (Na₂S) for 5 minutes, wherein the pre-adsorbed Pb²⁺ ions react with S²⁻ ions to form PbS. Then, the electrodes were rinsed with DI water and ethanol and dried under N₂ gas. These two dipping procedures

constitute one cycle, and two cycles were applied. Then, CdS was sensitized for five cycles using an aqueous solution of 0.1 M cadmium acetate dihydrate and 0.1 M Na₂S to achieve good adsorption over the PbS/TiO₂ photo-anode.

Finally, two cycles of ZnS passivating layers were coated over the CdS/PbS sensitized photo-anodes by the SILAR method using an aqueous solution of 0.1M Zn(NO₃)₂ and 0.1M(Na₂S), and each is dipped for 5min per cycle and washed several times, dried, and used for the fabrication of QDSSCs. The ZnS can proficiently cover the bare TiO₂/TiO₂/MgO, TiO₂/Al₂O₃ and TiO₂/MgO/Al₂O₃ and TiO₂/Al₂O₃/MgO and QDs, resulting in strong inhibition of the electron leakage from either the QDs or TiO₂ to the electrolyte.

2.3. Fabrication of CuS counter electrodes

CBD is a modest and easy method for preparing the metal sulfide CE and FTO substrate. Prior to deposition, the FTO samples were cleaned ultrasonically using acetone, ethanol and DI water for 10 minutes each. The prepared substrates were dried with N₂ gas. A CuS aqueous solution was prepared using 0.1 M CuSO₄·5H₂O and 0.4 M Na₂S₂O₃ as source of Cu²⁺ and S²⁻ ions, respectively. 0.4 M CH₄N₂O was used as a reagent for depositing CuS thin films. The substrates were then dipped horizontally into the solutions of CuS and kept in a hot air oven at 65 °C for about 2 h. The CuS-coated films were washed several times with DI water and ethanol.

2.4 Assembly of the QDSSCs

The photo electrodes (Bare TiO₂, TiO₂/MgO, TiO₂/Al₂O₃, TiO₂/Al₂O₃/MgO and TiO₂/MgO/Al₂O₃) sensitized with PbS/CdS and the CEs (CuS) were assembled and sealed in layers using a transparent 50 mm hot melt sealing sheet (double sheet of SX 1170-25, Solaronix). The polysulfide electrolyte was injected through a pin-hole made in the CE. The cells were left for a few hours to complete the diffusion of electrolyte within the photo-anode and the cells were tested under one sun illumination (AM 1.5 G, 100 mW cm⁻²).

2.5 Characterizations

The surface morphology of the thin films was characterized using field emission scanning electron microscopy (FE-SEM, S-4200, Hitachi) equipped with energy dispersive X-ray spectroscopy (EDS)

at an operating voltage of 15 kV to determine the elemental composition at the Busan KBSI. X-ray photoelectron spectroscopy (XPS, VG Escalab 250) was equipped with a hemispherical energy analyzer using mono-chromated Al K α radiation. QD adsorption was measured by UV-Vis spectroscopy (Mecasys OPTIZEN 3220UV) over the wavelength range, 400 to 800 nm. A source meter (Keithley 2400) was used to analyze the I-V characteristics under 1 sun illumination (100 mW/cm², AM 1.5). The internal resistance of the QDSSCs at room temperature was measured by electrochemical impedance spectroscopy (EIS; Biologic SP-150) at frequencies ranging from 100 mHz to 500 kHz. The applied bias voltage and AC amplitude were set to the V_{oc} of the QDSSCs and 10 mV, respectively. The electrical impedance was characterized using Nyquist and Bode plots. The surface roughness of the substrates prepared using SILAR was characterized by atomic force microscopy (JPK NanoWizard II AFM, JPK instruments, 158 Berlin, Germany) at a scan rate of 0.8 Hz in the contact mode.

3. RESULTS AND DISCUSSION

The operating mechanism of the proposed solar cells based on double coating barrier layer TiO₂/MgO/Al₂O₃ is shown in Fig. 2. The PbS and CdS mainly absorb visible light, generating photo-excited electron-hole pairs. After that, the electrons that were photo-excited on the CdS/PbS sensitizers were effectively transported to Al₂O₃, MgO and to TiO₂ through the cascade type-II band structure and holes stimulated in the opposite direction through the valence bands, finally oxidizing the polysulfide intermediary.

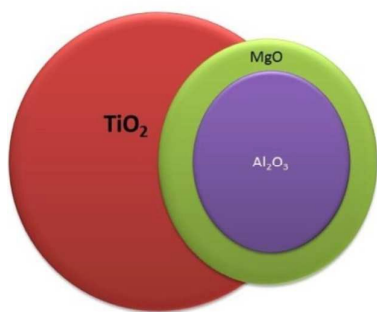


Fig. 2 Schematic diagram of double barrier layer

Metal oxides on TiO₂ have been proven to be a good barrier layer for reducing electron recombination at the TiO₂/QD/electrolyte

interface. Overall, the barrier layer on the surface of TiO₂ can improve the photovoltaic performance of the QDSSCs.

3.1 Structural and morphological studies

The SEM image in Fig. 3 shows the result of different barrier layers of MgO, Al₂O₃, MgO/Al₂O₃ and Al₂O₃/MgO on the surface of TiO₂. The TiO₂ film in Fig. 3a is composed of nano particles with average diameters in the range of ~14 to 24 nm. Fig. 3b and 3c shows the deposition of MgO and Al₂O₃ on the surface of TiO₂ with an average diameter of ~12 to 24 nm. The thickness in the photo-anodes was confirmed by cross-sectional view of SEM, and the results are shown in Fig. S1 of ESI.†

The Fig. 3d and e shows the high and low magnification SEM image of TiO₂/MgO/Al₂O₃ on TiO₂, the primer of MgO/Al₂O₃ shows the filling of pores in the TiO₂ whereas for Al₂O₃/MgO it is partially filled (Fig. 3f). The combination of MgO and Al₂O₃ nanoparticles in TiO₂ can fill the pores and facilitates the penetration of the electrolyte. The sample in Fig. 3d demonstrates that the high surface coverage of the barrier layer on TiO₂ increases with MgO coating. The Fig. 3f shows that the Al₂O₃/MgO particles had uniformly distributed on TiO₂ surface but it shows extremely large particle size compared to TiO₂/MgO/Al₂O₃ film. One recent study reported that high root-mean-square (RMS) roughness and too large particles might decrease the coverage on TiO₂ film and increase the series resistance of the whole electrode.⁵³ As seen in Fig. 3d, when the MgO and Al₂O₃ was deposited on the TiO₂ surface, there are many nanoparticles and these particles were interconnected together and covered the TiO₂ nanoparticles completely. These complete coverage of the TiO₂ with MgO and Al₂O₃, which would lead to strong adhesion between the material and FTO substrate. However, the improved surface morphology could extend the absorption in the visible and near IR regions of solar light. The elements in the photo-anodes were confirmed by EDX, and the results are shown in Fig. S2 of ESI.† The surface roughness of the PbS/CdS film, high-resolution tapping-mode atomic force microscopy (AFM) was carried out. The 2-dimensional (2D) and 3-dimensional (3D) images are shown in Fig. S3 of ESI.†

Journal Name

ARTICLE

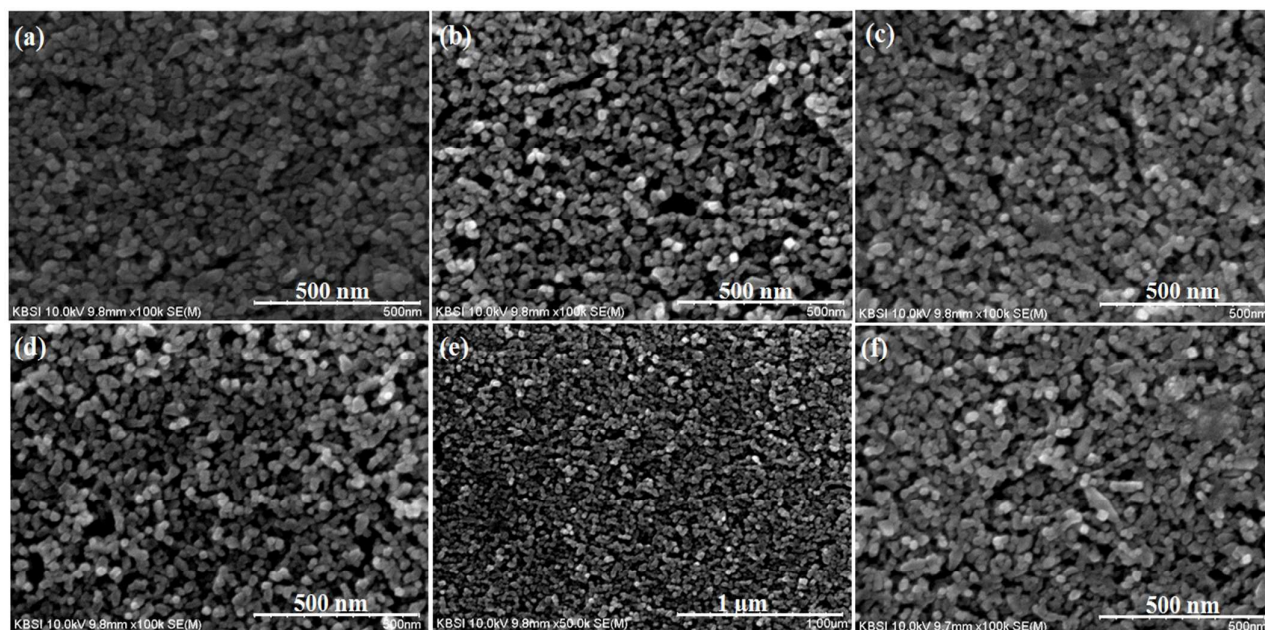


Fig. 3 SEM images of (a) TiO_2 , (b) TiO_2/MgO , (c) $\text{TiO}_2/\text{Al}_2\text{O}_3$, (d) and (e) high and low magnification images of $\text{TiO}_2/\text{MgO}/\text{Al}_2\text{O}_3$ and (f) $\text{TiO}_2/\text{Al}_2\text{O}_3/\text{MgO}$ images.

The presence of MgO and Al_2O_3 on the surface of TiO_2 is shown in Fig. 4 using XPS, which is used to measure the composition and chemical bond configuration. Fig. 4 (a and b) shows the binding energy peaks appeared at 50 eV ($\text{Mg}2p$) and 74 eV ($\text{Al}2p$) respectively indicating the formation of MgO and Al_2O_3 layer on TiO_2 film which is in well agreement with previous reports.^{54,55} Fig. 4c shows the $\text{O}1s$ and $\text{Ti}2p$ XPS spectra of the bare and double coated barrier layer on TiO_2 films, respectively. $\text{Ti}2p$ binding energies of ~ 464.5 and 458.7 eV are attributed to the $\text{Ti}2p$ 1/2 and $\text{Ti}2p$ 3/2, respectively which is shown in Fig. S4 of ESI.† An additional peak was observed at the higher energy side, which indicates the surface of hydroxyl (OH) groups with $\text{MgO}/\text{Al}_2\text{O}_3$ coating on TiO_2 . The increased number of hydroxyl groups of the metal oxide materials on the TiO_2 surface forms interfacial bonding with the carboxylic group of the QDs. The intensity of $\text{Ti}2p$ bands slightly decreased with the presence of insulating oxides (Fig. S4 of ESI. †).

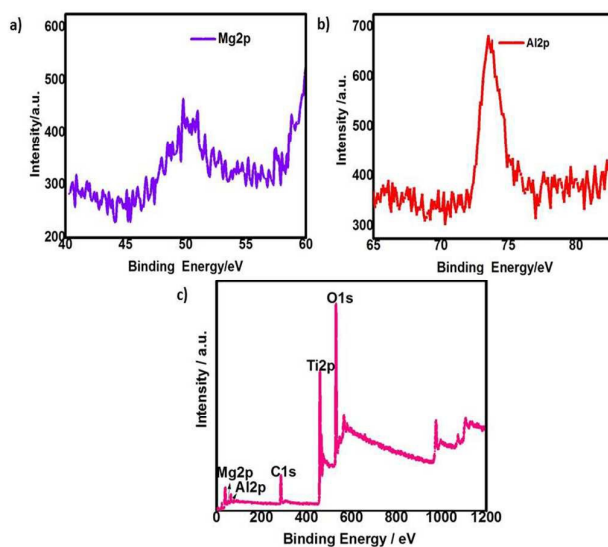


Fig. 4 XPS spectra of a) Mg (b) Al and (c) $\text{TiO}_2/\text{MgO}/\text{Al}_2\text{O}_3$.

In Fig. 5, the characteristic peaks of Ti, O, Al, Mg, Pb, Cd, Zn, S, are all shown. The Pb 4f and Cd 3d peak appears at a binding energy of 405.13 eV and 137.8 eV and reacts with S to form PbS and CdS. The binding energy peaks of Zn 2p_{3/2} are observed at 1022.37 eV.

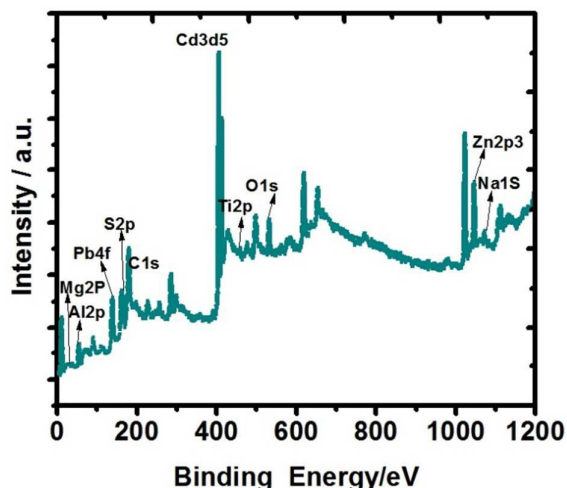


Fig.5 XPS spectra of TiO₂/MgO/Al₂O₃ sensitized PbS/CdS QDs.

3.2 Optical properties

As shown in Fig. 6, the TiO₂/MgO/Al₂O₃ showed the highest absorbance. The absorbance of the other double coated layers on the TiO₂ films was higher than that of single coated layer on TiO₂ and bare TiO₂. The increased absorbance was attributed to the higher IEP value.

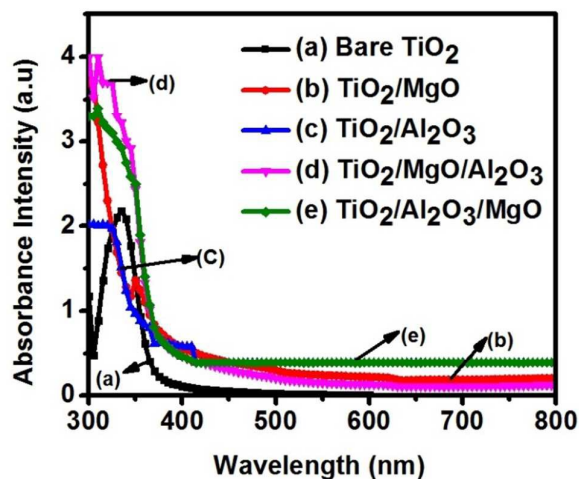


Fig. 6 UV-vis absorption spectra for (a) Bare TiO₂, (b) TiO₂/MgO, (c) TiO₂/Al₂O₃ and (d) TiO₂/MgO/Al₂O₃ and (e) TiO₂/Al₂O₃/MgO.

When an insulating oxide with a high IEP is coated on TiO₂ films, TiO₂ becomes negatively charged and attracts QDs due to the

opposite surface charge and carboxylate linkage of QDs.⁶⁵ MgO and Al₂O₃ have a higher IEP than TiO₂. Larger differences in the IEP cause significant enhancement in adsorption by QDs and a larger J_{sc}. The addition of an MgO over layer improved the absorbance because of the large difference in the IEP of TiO₂ and MgO. The IEP and band gap values are shown in Table 1.

Table 1 Band gap and isoelectric point (IEP) of TiO₂, MgO and Al₂O₃.

Name	Band Gap	IEP
TiO ₂	3.2~3.3	5.8
MgO	7.8	~12
Al ₂ O ₃	8.8	~9

3.3 Performance of QDSSCs with barrier layer on TiO₂

3.3.1. Photovoltaic analysis

The ultimate performance of the devices is studied. Fig. 7 shows the current versus voltage (J-V) curves of QDSSCs under one sun illumination. Photovoltaic parameters like V_{oc} (Open circuit voltage), J_{sc} (Current density), fill factor (FF), and total energy conversion efficiency (η) are listed in Table 2. Single and double coated barrier layers on the TiO₂ films results in an increase in the cell parameters. The increase in J_{sc} is observed upon increasing QD absorption and the increase in V_{oc} from 0.56 V to 0.61 V results from a shift of the conduction band because of the insulating oxide coating.

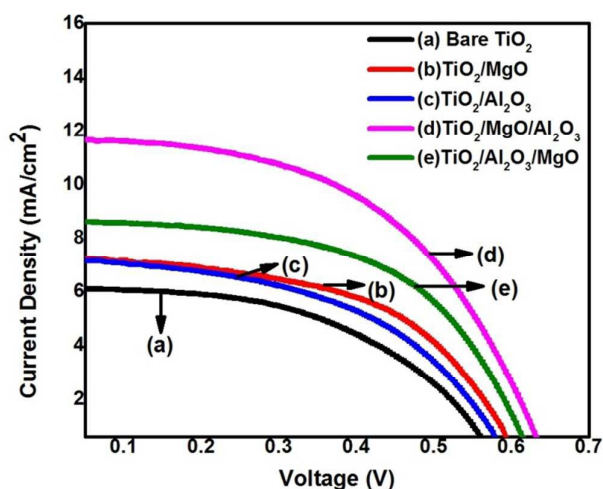


Fig.7 Photo-current density–voltage (J–V) characteristics of (a) Bare TiO₂, (b) TiO₂/MgO, (c) TiO₂/Al₂O₃ and (d) TiO₂/MgO/Al₂O₃ and (e)

TiO₂/Al₂O₃/MgO in QDSSCs with CuS counter electrodes and polysulfide electrolyte.

Table 2 Summary of the photovoltaic properties of Bare TiO₂, TiO₂/MgO, TiO₂/Al₂O₃ and TiO₂/MgO/Al₂O₃ and TiO₂/Al₂O₃/MgO in QDSSCs with CuS counter electrodes and polysulfide electrolyte.

Condition	V _{oc}	J _{sc}	FF	η(%)
Bare TiO ₂	0.56	6.6	0.51	1.95
TiO ₂ /MgO	0.58	7.93	0.53	2.56
TiO ₂ /Al ₂ O ₃	0.57	7.91	0.51	2.29
TiO ₂ /MgO/Al ₂ O ₃	0.63	11.40	0.56	3.25
TiO ₂ /Al ₂ O ₃ /MgO	0.61	9.76	0.53	3.18

A significant increase was also attained with a double coating because they show a big increase in V_{oc} and FF. This can be attributed to the formation of an effective barrier layers on the TiO₂ surface, indicating that the single and double layer itself worked as an effective barrier layer on TiO₂ electrode and increases the electron attentiveness at V_{oc}. The conversion efficiency of MgO/Al₂O₃ coated TiO₂ increased from 1.95% to 3.25% improvement compared to bare TiO₂. The result shows that the TiO₂/MgO/Al₂O₃ barrier layer for PbS/CdS acts as an efficient layer between the electrolyte and the TiO₂ surface, significantly improving the electron lifetime and leading to improved photovoltaic performance. The flow of electrons is through Al₂O₃, MgO and then to TiO₂ which reduces the recombination. The produced photo-electrons are expected to transfer to the electrolyte and combine with S_n²⁻ to form nS²⁻ to promote redox reactions in the electrolyte which is shown in Fig. 8.

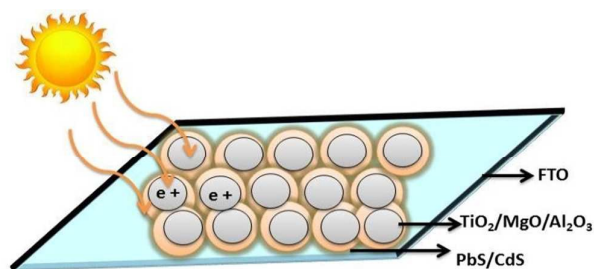


Fig. 8 Mechanism for the supply of photo electrons from the QDs.

3.3.2. Electrochemical impedance studies

Electro-chemical impedance spectroscopy (EIS) is a powerful tool for characterizing the performance of each component of QDSSCs, and it is used to investigate the interior resistance and charge transfer kinetics of QDSSCs. The Nyquist plots of QDSSCs Bare TiO₂, TiO₂/MgO, TiO₂/Al₂O₃ and TiO₂/MgO/Al₂O₃ and TiO₂/Al₂O₃/MgO photo-anodes were measured under a simulated light source of 100 mW cm⁻². The plots were analyzed using Z-view software with an equivalent circuit as shown in Fig. 9. The EIS investigation of the QDSSCs provides valuable information for understanding the photovoltaic parameters of J–V curves. EIS spectra of QDSSCs containing a liquid electrolyte exhibit three semicircles in the Nyquist plot. The starting point of the first semicircle is the series resistance R_s, which is the transport resistance of FTO and all resistances outside of the cell. The first semi-circle in the Nyquist plot contains the recombination resistance at the CE/electrolyte interface (R_{CE}), which is parallel to the CE capacitance (C_{CE}). The second semi-circle (middle frequency circle) is the charge transfer resistance (R_{ct}) at the TiO₂/QDs/electrolyte interface, which is parallel to the corresponding chemical capacitance (C_μ). In this study, second semi-circles are used to study the effect of the barrier layers as it is directly related to the charge transport and recombination resistance in the TiO₂ network. Insulating oxides can function as barrier layers for both electron injection and charge recombination reaction. The low frequency semi-circle (third semi-circle) is the Warburg diffusion (Z_w) in the electrolyte. Approximately near R_s values were obtained for all Nyquist plots in because of the identical CE (FTO/CuS).

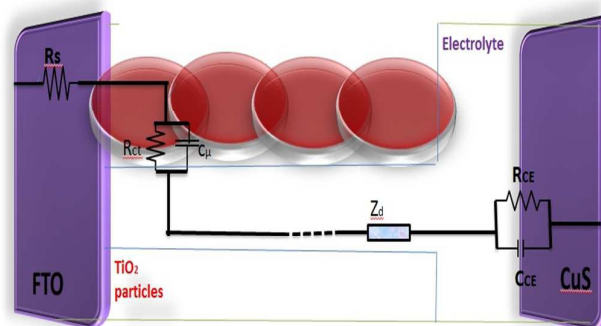


Fig.9 Equivalent circuit diagram of QDSSC.

The corresponding Nyquist plots for the frequency range of 100 mHz–500 kHz are shown in Fig.10. The parameters obtained from the EIS analysis are summarized in Table 3. The change in R_{CE} could be attributed to the property alteration of the redox polysulfide using similar CuS electrodes. The R_{CE} values of Bare TiO_2 , TiO_2/MgO , $\text{TiO}_2/\text{Al}_2\text{O}_3$ and $\text{TiO}_2/\text{MgO}/\text{Al}_2\text{O}_3$ and $\text{TiO}_2/\text{Al}_2\text{O}_3/\text{MgO}$ were found to be 3.97, 2.89, 3.54, 1.84 and 2.54 Ω respectively. The R_{ct} value of $\text{TiO}_2/\text{MgO}/\text{Al}_2\text{O}_3$ (8.7 Ω) which is lower than that of Bare TiO_2 (60.4 Ω), TiO_2/MgO (12.4 Ω), $\text{TiO}_2/\text{Al}_2\text{O}_3$ (27.9 Ω), $\text{TiO}_2/\text{Al}_2\text{O}_3/\text{MgO}$ (10.2 Ω). The low R_{ct} value suggests that the $\text{MgO}/\text{Al}_2\text{O}_3$ configuration provides better electron transport in the photo-anode by suppressing the recombination when the $\text{MgO}/\text{Al}_2\text{O}_3$ layer passivizes on the surface of TiO_2 . 56 $\text{MgO}/\text{Al}_2\text{O}_3$ coated TiO_2 showed the lowest resistance among the single and double coating layers, which indicates that the charge transfer resistance is reduced significantly by the $\text{MgO}/\text{Al}_2\text{O}_3$ barrier layer. The Z_w value (1.5 Ω) of the $\text{MgO}/\text{Al}_2\text{O}_3$ indicates improved electrolyte diffusion, expedites faster mass transport of the electrons, and increases the enactment of the QDSSCs. These results propose that, it allows the electron injection through tunneling with an ultrathin layer of insulating oxide. The chemical capacitance (C_μ) mostly designates the injection and accretion of electrons into the photo-anodes. The capacity to accrue electrons mainly depends on the conduction band position, as in Eqn (1): ^{57,58}

$$C_\mu = \frac{q^2}{K_B T} e \left[\frac{\alpha}{K_B T} (E_{Fn} - E_{cb}) \right] \quad (1)$$

Table 3 Summary of EIS results for Bare TiO_2 , TiO_2/MgO , $\text{TiO}_2/\text{Al}_2\text{O}_3$ and $\text{TiO}_2/\text{MgO}/\text{Al}_2\text{O}_3$ and $\text{TiO}_2/\text{Al}_2\text{O}_3/\text{MgO}$ in QDSSCs with CuS counter electrodes and polysulfide electrolyte.

Condition	$R_s(\Omega)$	$R_{CE}(\Omega)$	$R_{ct}(\mu\Omega)$	$C_\mu(\mu\text{F})$	$Z_w(\Omega)$
Bare TiO_2	11.76	3.97	60.4	7771	12.5
TiO_2/MgO	9.45	2.89	12.4	8514	8.9
$\text{TiO}_2/\text{Al}_2\text{O}_3$	10.38	3.54	27.9	7329	10.9
$\text{TiO}_2/\text{MgO}/\text{Al}_2\text{O}_3$	8.1	1.84	8.7	9285	1.5
$\text{TiO}_2/\text{Al}_2\text{O}_3/\text{MgO}$	8.9	2.54	10.2	8664	7.6

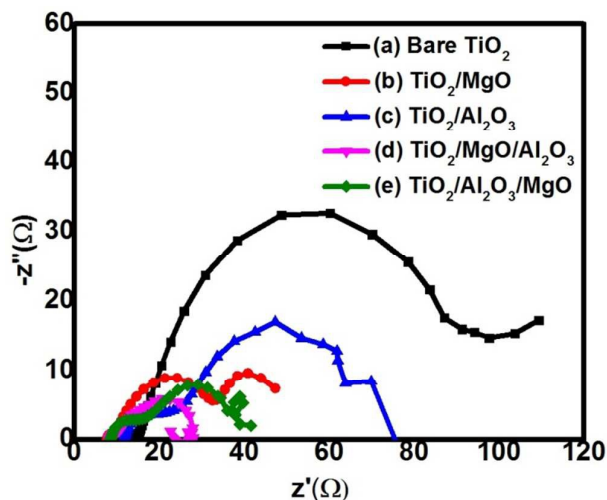
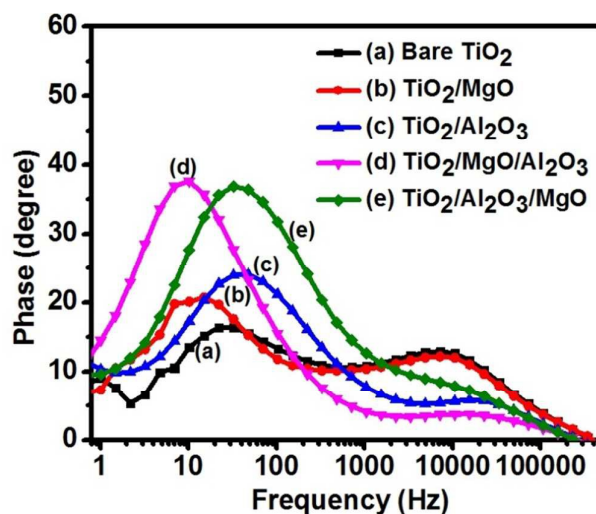
**Fig. 10** EIS spectra of Bare TiO_2 , TiO_2/MgO , $\text{TiO}_2/\text{Al}_2\text{O}_3$ and $\text{TiO}_2/\text{MgO}/\text{Al}_2\text{O}_3$ and $\text{TiO}_2/\text{Al}_2\text{O}_3/\text{MgO}$ in QDSSCs with CuS counter electrodes and polysulfide electrolyte.

Fig. 11 shows Bode phase diagram obtained from the EIS measurements, which supports the electron lifetime for the TiO_2 films. According to the EIS model, the electron lifetime before the recombination (τ_r) can be estimated using eqn (2) using the Bode plot.

$$[\tau_r = 1/(2\pi f_{\max})] \quad (2)$$

**Fig. 11** Bode phase-diagrams of Bare TiO_2 , TiO_2/MgO , $\text{TiO}_2/\text{Al}_2\text{O}_3$ and $\text{TiO}_2/\text{MgO}/\text{Al}_2\text{O}_3$ and $\text{TiO}_2/\text{Al}_2\text{O}_3/\text{MgO}$ in QDSSCs with CuS counter electrodes and polysulfide electrolyte.

The τ values obtained for Bare TiO_2 , TiO_2/MgO , $\text{TiO}_2/\text{Al}_2\text{O}_3$ and $\text{TiO}_2/\text{MgO}/\text{Al}_2\text{O}_3$ and $\text{TiO}_2/\text{Al}_2\text{O}_3/\text{MgO}$ in QDSSCs were 98, 105, 129, 296, and 218 ms respectively. The increased electron lifetime in $\text{TiO}_2/\text{MgO}/\text{Al}_2\text{O}_3$ supports the reduction of back-reaction for the injected electrons with a polysulfide electrolyte. The $\text{MgO}/\text{Al}_2\text{O}_3$ layer effectively acted as barrier on the surface of the TiO_2 and hence reduced the recombination.

In the case of QDSSCs system, the barrier layer can effectively reduce the backward reaction at the FTO/polysulfide electrolyte interface. It is clear from Fig. 12 the IPCE measurement shows the maximum value at a wavelength of 550 nm. At this wavelength, an increase in IPCE was observed from 15 to 20 % after the treatment of TiO_2 with $\text{MgO}/\text{Al}_2\text{O}_3$ QDs electrodes. This increase in IPCE leads to the increase in the charge collection which leads to increase of photo injected electrons in TiO_2 conduction band. The metal oxide blocking layer can remarkably decrease the recombination resulting in higher V_{OC} and J_{SC} compared with the bare TiO_2 cell. The J_{SC} values calculated from integration of the IPCE spectra for bare TiO_2 (6.6 ± 0.1), TiO_2/MgO (7.93 ± 0.55), $\text{TiO}_2/\text{Al}_2\text{O}_3$ (7.91 ± 0.58), $\text{TiO}_2/\text{MgO}/\text{Al}_2\text{O}_3$ (11.40 ± 0.49) and $\text{TiO}_2/\text{Al}_2\text{O}_3/\text{MgO}$ (9.76 ± 0.42) were well matched with J_{SC} obtained from the J-V measurements, considering the common error of 5–10%.

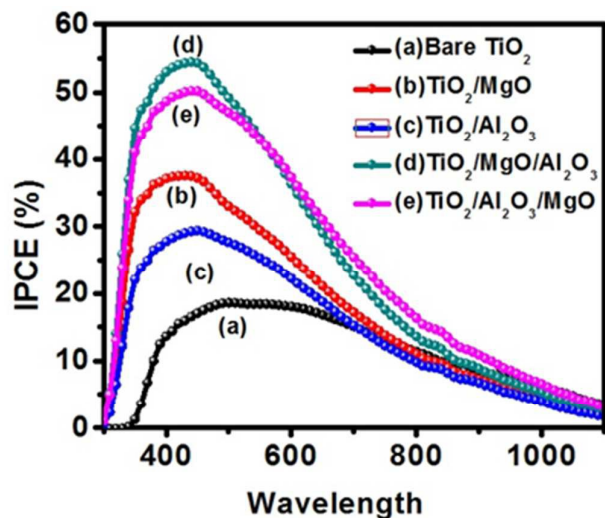


Fig. 12 IPCE spectra for (a) Bare TiO_2 , (b) TiO_2/MgO , (c) $\text{TiO}_2/\text{Al}_2\text{O}_3$ (d) $\text{TiO}_2/\text{MgO}/\text{Al}_2\text{O}_3$ and (e) $\text{TiO}_2/\text{Al}_2\text{O}_3/\text{MgO}$ in QDSSCs with CuS counter electrodes and polysulfide electrolyte

Fig. 13 shows the impedance spectra for the Bare TiO_2 , TiO_2/MgO , $\text{TiO}_2/\text{Al}_2\text{O}_3$ and $\text{TiO}_2/\text{MgO}/\text{Al}_2\text{O}_3$ and $\text{TiO}_2/\text{Al}_2\text{O}_3/\text{MgO}$ under the dark condition with 0.7 V. The decrease in diameter under bias condition is due to the electrons injected into the conduction band of TiO_2 that recombine with the polysulfide electrolyte. Under the short circuit conditions, more number of injected electrons reaches the external circuit via the back contact, so the number of electrons returning to the redox couple is abridgedominously.⁵⁹ Therefore, the decrease of the lower frequency semicircle can be explained by the change of the number of electrons recombining with the electrolyte at the $\text{TiO}_2/\text{electrolyte}$ interface.

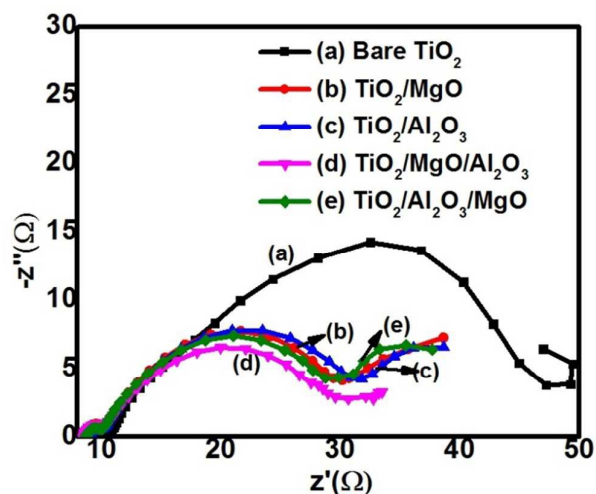


Fig. 13 EIS spectra of Bare TiO_2 , TiO_2/MgO , $\text{TiO}_2/\text{Al}_2\text{O}_3$ and $\text{TiO}_2/\text{MgO}/\text{Al}_2\text{O}_3$ and $\text{TiO}_2/\text{Al}_2\text{O}_3/\text{MgO}$ in QDSSCs with CuS counter electrodes and polysulfide electrolyte under dark condition.

The arc of the semicircle is closely related to the short circuit current, and expansion of the semicircle at lower frequency corresponds to a decrease in the short circuit current. The QDSSC based on $\text{TiO}_2/\text{MgO}/\text{Al}_2\text{O}_3$ and shows a smaller lower frequency than that based on Bare TiO_2 , TiO_2/MgO , $\text{TiO}_2/\text{Al}_2\text{O}_3$ and $\text{TiO}_2/\text{Al}_2\text{O}_3/\text{MgO}$ which may be due to the higher recombination of electrons with the polysulfide electrolyte. These results suggest that the internal resistance at the $\text{TiO}_2/\text{electrolyte}$ interface in the QDSSC is a crucial factor for the performance of the cell.⁶⁰ The Bare TiO_2 , TiO_2/MgO , $\text{TiO}_2/\text{Al}_2\text{O}_3$ and $\text{TiO}_2/\text{Al}_2\text{O}_3/\text{MgO}$ based QDSSCs showed reduced charge transfer resistance and chemical capacitance, which is due to its high recombination of electrons

with the electrolyte. This leads in reducing the electron injection and the shift in the Fermi level to the conduction band energy.⁶⁰

Fig. 14 shows photo-voltage decay plots and the electron lifetimes as a function of photo-voltage. The electron loss due to recombination can be monitored by measuring the open circuit voltage decay (OCVD) after switching off the light. It was observed that the OCVD of cell with the double coated barrier layers was much slower than that without the barrier layer. Slower decay results in the increased electron life-time. The optimized band gap and the appropriate combination of insulating oxide materials, such as MgO/Al₂O₃, effectively suppresses electron leakage and enhanced the cell performance with lower combination reactions of MgO and higher conduction band edge of Al₂O₃. The decreased electron lifetime of Bare TiO₂, TiO₂/Al₂O₃ and TiO₂/Al₂O₃/MgO electrodes indicates a higher charge recombination rate and lower charge collection efficiency than TiO₂/MgO/Al₂O₃.

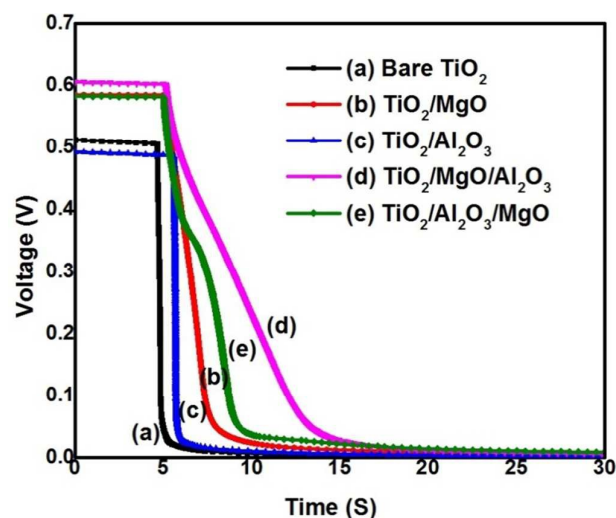


Fig. 14 Open-circuit voltage-decay of (a) Bare TiO₂, (b) TiO₂/MgO, (c) TiO₂/Al₂O₃ (d) TiO₂/MgO/Al₂O₃ and (e) TiO₂/Al₂O₃/MgO measurements after switching off the illumination of QDSSCs.

4 Conclusions

A single and double coated barrier layer was fabricated on the TiO₂ films using MgO and Al₂O₃ to reduce recombination reactions, and longer electron lifetime. The combination of insulating oxide materials (MgO/Al₂O₃) escalates the conversion efficiency. The double coated barrier layer had a more effective energy barrier than the single coating by improving the overall cell parameters. However, successive layers of PbS with CdS significantly enhances

photo-current. The quantum dot sensitized solar cell performance is enhanced which is attributed due to the better light harvesting ability of PbS quantum dots and makes large accumulation of photo-injected electrons in the conduction band of TiO₂. The large accumulation of photo-injected carriers in the conduction band of the photo-anode TiO₂/MgO/Al₂O₃ and lower recombination of photo-generated electrons with the electrolyte in were confirmed by impedance analysis. The enrichment in the photovoltaic performance with quantum-dot sensitization and metal oxides on TiO₂ is another breakthrough for achieving higher J_{sc} (11.40 mA cm⁻²), V_{oc} (0.63V) photo-conversion efficiency of 3.25%. This methodology can be extended to other metal oxides and different quantum dot sensitizers which opens path for further development of photovoltaic technology.

Acknowledgements

This research was supported by Basic Research Laboratory through the National Research Foundations of Korea funded by the Ministry of Science, ICT and Future Planning (NRF-2015R1A4A1041584). We would like to thank KBSI, Busan for SEM, XPS, EDX analysis.

References

- 1 F. Huang, D. Chen, X. Zhang, R. Caruso and Y. Cheng, *Advanced Functional Materials*, 2010, **20**, 1301-1305.
- 2 C. Chen, M. Wang, J. Li, N. Pootrakulchote, L. Alibabaei, C. Ngocle, J. Decoppet, J. Tsai, C. Gratzel, C. Wu, S. Zakeeruddin and M. Gratzel, *ACS Nano*, 2009, **3**, 3103-3109.
- 3 A. Kongkanand, K. Tvrđy, K. Takechi, M. Kuno and P. Kamat, *Journal of American Chemical Society*, 2008, **130**, 4007-4015.
- 4 C. Chang and Y. Lee, *Applied Physics Letters*, 2007, **91**, 053503.
- 5 H. Lee, M., Wang, P., Chen, D., Gamelin, S., Zakeeruddin, M. Gratzel and M. Nazeeruddin, *Nano Letters*, 2009, **12**, 4221-4227.
- 6 T. Li, Y. Lee and H. Teng, *Energy and Environmental Science*, 2012, **5**, 5315-5324.
- 7 M. Hanna, M. Beard and A. Nozik, *Journal of Physical Chemistry Letter*, 2012, **3**, 2857-2862.
- 8 R. S. Selinsky, Q. Ding, M. S. Faber, J. C. Wright and S. Jin, *Chemical Society Reviews*, 2012, **42**, 2963-2985.
- 9 P. V. Kamat, *Accounts of Chemical Research*, 2012, **45**, 1906-1915.
- 10 J. H. Bang and P. V. Kamat, *ACS Nano*, 2009, **3**, 1467-1476.

Journal Name

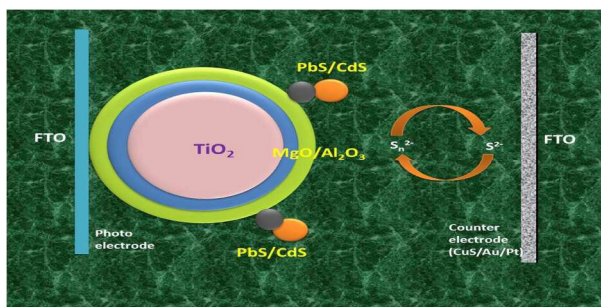
ARTICLE

- 11 X. Yu, B. Lei, D. Kuang and C. Su, *Journal of Material Chemistry*, 2012, **22**, 12058–12063.
- 12 K. G. U. Wijayantha, L. M. Peter and L. C. Otley, *Solar Energy Materials and Solar Cells*, 2003, **83**, 363–369.
- 13 N. Fuke, L. B. Hoch, A. Y. Kuposov, V. W. Manner, D. J. Werder, A. Fukui, N. Koide, H. Katayama and M. Sykora, *ACS Nano*, 2010, **4**, 6377–6386.
- 14 K. S. Leschkies, R. Divakar, J. Basu, E. E. Pommer, J. E. Boercker, C. B. Carter, U. R. Kortshagen, D. J. Norris and E. S. Aydil, *Nano Letters*, 2007, **7**, 1793–1798.
- 15 N. Balis, V. Dracopoulos, K. Bourikas and P. Lianos, *Electrochimica Acta*, 2013, **91**, 246–252.
- 16 Q. Shen, J. Kobayashi, J. Lina and T. Toyoda, *Journal of Applied Physics*, 2012, **103**, 084304.
- 17 P. K. Santra and P. V. Kamat, *Journal of American Chemical Society*, 2012, **134**, 2508–2511.
- 18 Y.-L. Lee and Y.-S. Lo, *Advanced Functional Materials*, 2009, **19**, 604–609.
- 19 N. Guijarro, J. M. Campina, Q. Shen, T. Toyoda, T. Lana-Villarreal and R. Gomez, *Physical Chemistry Chemical Physics*, 2011, **13**, 12024–12032.
- 20 C. Pejoux, S. Röhle, D. Cahen and G. Hodes, *Journal of Photochemistry and Photobiology A*, 2006, **181**, 306–313.
- 21 M. Nikumbh, V. Gore and R. B. Gore, *Renewable Energy*, 1997, **11**, 459–467.
- 22 A. Braga, S. Gimenez, I. Concina, A. Vomiero and I. M. Sero, *Journal of Physical Chemistry Letters*, 2011, **2**, 454–460.
- 23 J. B. Sambur, T. Novet and B. A. Parkinson, *Science*, 2010, **330**, 63–66.
- 24 B. R. Hyun, Y. W. Zhong, A. C. Bartnik, L. Sun, H. D. Abrun, F. W. Wise, J. D. Goodreau, J. R. Matthews, T. M. Leslie and N. F. Borrelli, *ACS Nano*, 2008, **2**, 2206–2212.
- 25 H. Lee, H. C. Leventis, S. J. Moon, P. Chen, S. Ito, S. A. Haque, T. Torres, F. Neuesch, T. Geiger, S. M. Zakeeruddin, M. Gratzel and M. Nazeeruddin, *Advanced Functional Materials*, 2009, **19**, 2735–2742.
- 26 D. Punnoose, S. S. Rao, S.-k. Kim and H.-J. Kim, *RSC Advances*, 2015, **5**, 33136.
- 27 C. Justin Raj, S. N. Karthick, S. Park, K. V. Hemalatha, S.-K. Kim, K. Prabakar and H.-J. Kim, *Journal of Power Sources*, 2014, **248**, 439–446.
- 28 I. Mora-Sero, S. Gimenez, F. Fabreat-Santiago, R. Gomez, Q. Shen, T. Toyoda and J. Bisquert, *Accounts of Chemical Research*, 2009, **42**, 1848–1857.
- 29 Z. Tachan, I. Hod, M. Shalom, L. Grinis, A. Zaban, *Physical Chemistry Chemical Physics*, 2013, **15**, 3841–3845.
- 30 T. Brennan, O. Trejo, K. Roelofs, J. Xu, F. Prinz, and S. Bent, *Journal of Material Chemistry*, 2013, **1**, 7566–7571.
- 31 K. Tsujimoto, D. Nguyen, S. Ito, H. Nishino, H. Matsuyoshi, A. Konno, G. Kumara and K. Tennakone, *Journal of Physical Chemistry C*, 2012, **116**, 13465–13471.
- 32 K. Roelofs, T. Brennan, J. Dominguez, C. Bailie, G. Margulis, E. Hoke, M. McGehee and S. Bet, *Journal of Physical Chemistry C*, 2013, **117**, 5584–5592.
- 33 V.V. Hoang, *Chemical Physics Research Journal*, 2011, **4**, 43–62.
- 34 A.E. Kestell and G.T. DeLorey, *Nova Science Publishers Inc*, New York, 2010, 213–254.
- 35 J.J. Wu, M.D. Hsieh, W.P. Liao, W.T. Wu, and J.S. Chen, *ACS Nano*, 2009, **3**, 2297–2303.
- 36 K. Lee, D. Kim, S. Berger, R. Kirchgeorg and P. Schmuki, *Journal of Material Chemistry*, 2012, **22**, 9821–9825.
- 37 T. Tachikawa and T. Majima, *Chemical Society Reviews*, 2010, **39**, 4802–4819.
- 38 Z. Hu, Q. Zhang, J. Gao, Z. Liu, J. Zhai and L. Jiang, *Langmuir*, 2013, **29**, 4806–4812.
- 39 Z. Zhang, L. Zhang, M.N. Hedhili, H. Zhang and P. Wang, *Nano Letters*, 2013, **13**, 14–20.
- 40 T. Brenna, J., Bakke, I., Ding, B., Hardin, W., Nguyen, R., Mondal, C., Bailie, G., Margulis, E., Hoke, A., Sellinger, M., McGehee and S. Bent, *Physical Chemistry Chemical Physics*, 2012, **14**, 12130–12140.
- 41 R. Ceylantekin, and C. Aksel, *Ceramics International*, 2012, **38**, 995–1002.
- 42 A. Keskin, M. Guerue, and D. Altiparmak, *Bioresource Technology*, 2008, **99**, 6434–6438.
- 43 A. Sinsarp, T. Manago, and H. Akinaga, *Journal of Magnetism and Magnetic Materials*, 2007, **310**, 693–695.
- 44 G.S. Lee, J.Y. Lee, Y.B. Cheon, K.B. Kim, J.J. Kim and S.H. Sohn, *Thin Solid Films*, 2011, **519**, 3037–3042.
- 45 R. Kim, Y. Kim and J.W. Park, *Thin Solid Films*, 2000, **376**, 183–187.

ARTICLE

Journal Name

- 46 M. Fujishima, H. Takatori and H. Tada, *Journal of Colloids and Interface Science*, 2011, **361**, 628–631.
- 47 J. Bandara, S.S. Kuruppu and U.W. Pradeep, *Colloids and Surfaces A: Physicochemical and Engineering Aspects*, 2006, **276**, 197–202.
- 48 L. Liu, C. Zhao, H. Zhao, D. Pitts and Y. Li, *Chemical Communication*, 2013, **49**, 3664–3666.
- 49 D. Arun Kumar, J. Alex Xavier, J. MerlineShyla and F.P. Xavier, *Journal of Material Science*, 2013, **48**, 3700–3707.
- 50 S. Wu, H. Han, Q. Tai, J. Zhang, S. Xu, C. Zhou, Y. Yang, H. Hu, B. Chen, B. Sebo and X.Z. Zhao, *Nanotechnology*, 2008, **19**, 215704-1–215704-6.
- 51 C. Mukherjee, T. Das, C. Mahata, C. K. Maiti, C. K. Chia, S. Y. Chiam, D. Z. Chi and G. K. Dalapati, *ACS Applied Materials and Interfaces*, 2014, **6**, 3263–3274.
- 52 Jae-Yup Kim, Soon Hyung Kang, Hyun Sik Kim, and Yung-Eun Sung, *ACS Langmuir*, 2010, **26**, 2864–2870.
- 53 S. S. Rao, I. K. Durga, T. S. Kang, S. K. Kim, D. Punnoose, C. V. M. Gopi, A. E. Reddy, T. N. V. Krishna, and Hee-Je Kim, *Dalton Trans.*, 2016, DOI: 10.1039/c5dt04887g.
- 54 P. Casey, G. Hughes, E. O'Connor, R. D. Long and P. K. Hurley, *Journal of Physics: Conference Series*, 2008, **100**, 042046.
- 55 I. Iatsunsky, M. Kempinski, M. Jancelewicz, K. Zaleski, S. Jurga and V. Smyntyna, *Vacuum*, 2015, **113**, 52–58.
- 56 S. S. Rao, I. K. Durga, C. V. V. M. Gopi, C. V. Tulasivarma, S. K. Kim and Hee-Je Kim, *Dalton Trans.*, 2015, **44**, 12852–12862.
- 57 C. J. Raj, S. N. Karthick, K. V. Hemalatha, M. K. Son, H. J. Kim and K. Prabakar, *Journal of Sol-Gel Science and Technology*, 2012, **62**, 453–459.
- 58 J. Bisquert, *Physical chemistry chemical physics*, 2003, **5**, 5360–5364.
- 59 T. Hoshikawa, M. Yamada, R. Kikuchi and K. Eguchi, *Journal of Electrochemical Society*, 2005, **152**, E68–E73.
- 60 Chandu V. V. M. Gopi, M. Venkata-Haritha, S-K Kim and H-J Kim, *Nanoscale*, 2015, **7**, 12552–12563.

Table of Contents (TOC)

A solar cell based on double coating electrode ($\text{MgO/Al}_2\text{O}_3$) on TiO_2 yielded excellent performance with efficiency (η) of 3.25%.